An open laboratory blade strike rig to evaluate the risk of injury and mortality to fish and to test passive sensors

Wolf Iring Kösters, Jeffrey A Tuhtan, Danil Efimov, Maarja Kruusmaa, Stefan Hoerner

Sustainable Energy Technologies and Assessments 81 (2025) 104427

Contents lists available at ScienceDirect

Sustainable Energy Technologies and Assessments

journal homepage: www.elsevier.com/locate/seta

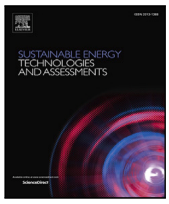

Original article

An open laboratory blade strike rig to evaluate the risk of injury and mortality to fish and to test passive sensors

Wolf Iring Kösters [a,b,*], Jeffrey A. Tuhtan [b], Danil Efimov [a], Maarja Kruusmaa [b], Stefan Hoerner [c,a]

[a] Laboratory of Fluid Dynamics and Technical Flows, Institute of Fluid Dynamics and Thermodynamics, Otto von Guericke University Magdeburg (OvGU), Universitaetsplatz 2, 39106 Magdeburg, Germany
[b] Centre for Biorobotics, Tallinn University of Technology (TalTech), Akadeemia tee 15A, 12618 Tallinn, Estonia
[c] Laboratory of Geophysical and Industrial Flows (LEGI), CNRS, G-INP, University Grenoble-Alpes, F-38000 Grenoble, France

ARTICLE INFO

Dataset link: https://github.com/ikoesters/srdatacombiner

Keywords:
Fish passage
Turbine passage
Fish-friendly turbine
Fish injury
Sensor probe

ABSTRACT

Hydropower is a key source of electricity that can negatively impact aquatic ecosystems. Fish passing downstream through hydropower facilities may face increased risks of injury and mortality from mechanical collisions with hydraulic structures and machinery. Laboratory tests provide a controlled environment to evaluate turbine blade strike risks, studying injury and mortality in live fish. Previous laboratory blade strike rigs vary substantially in design and implementation, lacking a standardized approach with controlled blade velocities for cross-comparable results. To address this, we propose an open laboratory blade strike test rig with electronically controlled blade velocities (1–10 m s^{-1}). In addition, rigid sensor tests were performed to investigate the recommendation that 95 g is suitable to assess the severity of the blade strike, which was exceeded at strike speeds as low as 1 m s^{-1}. This work is significant because it provides the hydropower, engineering and biological communities with the first open and standardized method to evaluate blade strikes on fish and sensor probes. The proposed test rig enables gathering biological threshold data to estimate injury and mortality to live fish, assessing turbine blade design for improved fish safety, and increasing sensor probe accuracy without relying on live fish field studies.

Introduction

Hydropower is a key source of electricity for base load power generation and plays a vital role in stabilizing electric grids, particularly in systems with a high share of renewable energy sources [1]. Despite the indisputable benefits of hydropower and the urgent need for resilient renewable energy infrastructure, the negative impacts of hydropower on river ecosystems has become increasingly evident, particularly on entrained fish [2,3], which can experience mortality rates exceeding the population's replacement rate, potentially leading to population collapse [4]. Hydropower has been identified as one driver behind a decline in migratory aquatic species through river fragmentation [5], affecting both potamodromous (solely living in fresh water) and diadromous (migrating between the sea and fresh water) fish species [6]. Many operators, manufacturers and authorities have made efforts to mitigate the environmental impact of hydropower in the last decades, and legislation puts increasing pressure on its operators by enforcing measures for safe fish passage as through the Water Framework Directive in the European Union [7]. The importance of these challenges is also reflected in the fact that fish safety is presented as a key feature in the innovative in-stream turbines over classical hydropower [8].

In spite of the associated environmental impacts, the number of hydroelectric plants continues to rise, with 3909 hydropower plants under development as of 2022, representing 9% of the total capacity installed to date [9]. Yet half of all hydroelectric power plants worldwide were constructed over 40 years ago and are due for modernization [10], providing an important opportunity to introduce new turbine designs to reduce their environmental impacts. Examples of innovative turbines include the minimum gap runner turbine [11], Alden turbine [11,12], the very low head turbine [13] and the restoration hydro turbine [14].

In some cases, bypasses can be built which provide fish the opportunity to migrate around hydroelectric facilities, including fishways, bypasses, and screens. However, such mitigation solutions, such as surface bypasses, may be difficult to evaluate across study sites due to

* Corresponding author at: Laboratory of Fluid Dynamics and Technical Flows, Institute of Fluid Dynamics and Thermodynamics, Otto von Guericke University Magdeburg (OvGU), Universitaetsplatz 2, 39106 Magdeburg, Germany.
E-mail address: wolf.koesters@ovgu.de (W.I. Kösters).

https://doi.org/10.1016/j.seta.2025.104427
Received 23 January 2025; Received in revised form 23 May 2025; Accepted 24 June 2025
Available online 17 July 2025

Nomenclature

Φ	Angular rotation
d_{rotor}	Rotor diameter
r	Coefficient of determination
s_{travel}	Length of relevant blade travel length
x_i	Peak acceleration magnitude value from a single experiment
X_{sv}	Array of peak acceleration magnitude values at one strike velocity
BDS	Barotrauma detection system
CAD	Computer-aided design
CFD	Computational Fluid Dynamics
CV	Coefficient of variation
EPRI	Electric Power Research Institute
HBET	Hydropower Biological Evaluation Toolset
L/t ratio	Fish length to blade thickness ratio
MAD	Mean absolute deviation
MSWR	Minimum strike window requirement
ORNL	Oak Ridge National Laboratory
PC	Polycarbonate
PCB	Printed circuit board
PU	Polyurethane
RAPID	Robust Autonomous Pressure and Inertial Device
RETERO	Project name
RPM	Revolutions per minute

a lack of standardized performance criteria [15]. Recent field studies have shown that at some sites, between 35–88 % of fish passed through the turbine despite the presence of bypasses and the installation of fine screens [16]. Additionally, such structures can result in elevated predation rates at these choke points [17].

Once entrained in a turbine, fish mortality is typically high: in a study summarizing 249 experiments reported in 91 studies on downstream migration through hydropower turbines in North America and Europe, Radinger et al. [18] estimated the average mortality rate at 22.3 %. Even sites employing new turbine designs, such as the previously mentioned very low head turbine, can still result in considerable passage mortality [19]. In cases where the mortality rates from turbine passage are higher than the reproduction rate, populations may face a risk of collapsing. To estimate large-scale impacts, ecological risk screening at the population level can be carried out using the European Fish Hazard Index (EFHI), developed by Van Treeck et al. [4].

Live fish tests remain the state-of-the-art method for assessing and quantifying the risk of injury and mortality to fish during downstream turbine passage, which is reflected in the current draft for a European standard [20] and the national Dutch standard [21] from 2020. Furthermore, such assessments may be mandated as a consequence of national regulations and policies such as the European Water Framework Directive [7], as hydropower operators are required to meet legal obligations related to their ecological impacts. A key advantage of using live fish is their ability to account for all sources of mechanical injury and mortality during passage, including barotrauma, shear, and collision events such as pinching, grinding, and blade strikes [22,23]. However, live fish tests can be prohibitively expensive for small hydropower plant operators and are subject to increasing ethical concerns, as demonstrated by the restriction of such tests in Switzerland via the Animal Welfare Act [24] and the Animal Experimentation Ordinance [25]. Additionally, live fish field tests only provide the cumulative outcome of physical damage, making it difficult or impossible to infer the precise locations within the hydraulic structure and machinery where damages occur, and can be highly species-, size-, life stage-, site- and operation point dependent.

To address the limitations and shortcomings of live fish testing, researchers have developed numerical models to investigate the hydraulic conditions to which fish would be exposed [26–30], which is a valuable guide for the design of environmentally enhanced turbines [31] and pumps [32,33]. However, the flow field in hydraulic machinery is extremely complex, and computational fluid dynamics (CFD) models require physical validation. Furthermore, most current CFD models do not take fish swimming activity into account.

Sensor probes, which were first patented by researchers at the US Army Corps [34] to study fish behavior near hydropower intakes. Subsequently, the ‘Sensor Fish’ was developed by Carlson and Duncan [35] for turbine passage studies and was later enhanced by Deng et al. [36] and Deng et al. [37] to measure the physical environment, focusing primarily on pressure, acceleration and rotational rate. These measurements have since been used in several studies to assess dam hydraulic conditions in situ (e.g. [38–42]) and to investigate new or unconventional turbine designs [43–45]. They have also been used to estimate the risk of barotrauma in juvenile salmon [46], including a recent improvement which includes a dynamic model of swim bladder size as proposed by Kerr et al. [47].

A significant limitation of passive sensor probe devices is their inability to account for fish behavior, which has been demonstrated to substantially influence outcomes. Geiger et al. [48] investigated the influence of behavior of river trout (*Salmo trutta fario*) on turbine passage mortality by conducting experiments in a model laboratory turbine. They modified fish behavior by either sedating the fish or using a device that induced an electric field at the turbine intake. Their findings demonstrated an approximately 50% reduction in mortality rates for fish of 15 cm and 29 cm length in the electric field group compared to the control group. Sedation also reduced mortality, although its effect was smaller yet still significant. Additionally, Vowles and Kemp [49] studied the influence of lighting conditions on the passage of brown trout (*Salmo trutta*) and reported substantial delays due to avoidance behaviors triggered by light exposure. Nonetheless, passive sensor probes are increasingly employed to quantify hydrodynamic parameters beyond their original application in hydraulic machinery, supporting broader fish-protection research efforts — such as recent investigations into closed-conduit systems [50].

To establish an equivalent model for shear events, Deng et al. [51] measured the acceleration and subsequent mortality of smolts subjected to shear flow induced by a high-velocity water jet. High-speed cameras measured the whole-body movement of the fish, from which velocity, acceleration, and jerk were calculated and compared to respective mortality for each velocity of the water jet. Based on these experiments, they classified events by peak acceleration magnitude of the sensor probe into three risk categories: low (25–50 g), medium (50–95 g), and high (greater than 95 g) for shear and collision events, distinguished by their magnitude and duration [38]. Events with a duration of less than 7.5 ms, measured as at least 70% of the maximum value, were classified as collisions, while those exceeding 7.5 ms were considered shear events. In addition to the development of this method [51], further information can be obtained in Richmond et al. [52], where fish and sensors were subjected to the same shear conditions and fish mortality was correlated with the full-body sensor acceleration. The results of this study were presented as a logistic regression with confidence intervals for the probability of minor and major injuries. However, the interpretation of the boundaries for these classes remains unclear as in one shear case (slow fish – fast water) 95 g the logistic regression curve already predicts major injuries with a mean probability close to 100%. Finally, these thresholds were also applied for collision events, even though the sensor did not experience a shock event during shear flow in the same way as it would have experienced during a collision. Thus, the use of the 95 g threshold may lead to an overestimation

of the severity of collision events as highlighted by Bercovitz et al. [53]. To further investigate acceleration thresholds, the authors have presented preliminary results from laboratory strike rig experiments related to acceleration maxima on 10 cm long 2.5 cm outer diameter plastic cylindrical sensors [54].

Currently, the acceleration-threshold concept, based on Richmond et al. [52] and introduced in Deng et al. [38], remains as the most common methodology to assess the severity of blade strike events; however an alternative based on the kinetic energies of translation and rotation was proposed in Pauwels et al. [44]. The acceleration-threshold model of Deng et al. [38] is used by the commercial software "Hydropower Biological Evaluation Toolset" (HBET) [55] accompanying the ATS Sensor Fish [37] to evaluate the passage through hydro-structures. With over 520 publications (using Google Scholar with the keyword "Sensor Fish"), this device can be estimated as the most widely used and is the only commercialized sensor model. It samples data at 2 kHz using a 3-axis gyroscope, a pressure sensor, and a 3-axis accelerometer with a measurement range of up to 112.5 g. The device has a cylindrical shape with a diameter of 24.5 mm, a length of 90 mm, and is neutrally buoyant at 43 g [36] Recent publications using the 95 g rule for collisions [41,43,45,56] illustrate its widespread application, despite a clear validation case of the 95 g criteria based on field or strike rig lab studies.

To address the absence of a biological response model for turbine blade strikes on fish, data from existing blade strike experiments conducted over the past three decades [14,57–62] can be used to link relative blade strike velocity with injury and mortality.

These blade strike rigs can be broadly categorized by their design as either electric motor-powered or spring-driven, and by their motion as either rotary or linear. The original design by Turnpenny et al. [57] featured a spring-driven blade with linear motion, although detailed replication information is scarce [63]. In 2007, Hecker et al. [64] employed a motor-powered linear motion rig, subsequently called Alden rig, identifying a key relationship between the blade-to-fish length ratio and mortality, and establishing the now-standard semicircular blade shape. A decade later, Bevelhimer et al. [63] introduced a compact spring-powered rig with rotary motion, subsequently called ORNL rig. Their extensive research on strike angle, location, fish rotation, and species impact on mortality was later compiled by Saylor et al. [65]. Most recently, Meng et al. [62] presented a rig similar to the ORNL rig design.

Ideally, these experiments can be replicated with sensors in order to infer the risk of injury and mortality from sensor measurements, following a potential methodology illustrated in Fig. 1. In the figure, the model only accounts for blade speed, omitting the L/t ratio (fish length to blade thickness ratio), which has been identified as another critical factor in blade strike mortality [64]. However, just as the model correlates strike velocity with acceleration, the L/t ratio can be incorporated the same way. The idea of performing simulated blade strikes on sensor probes to infer a mortality risk for fish, although not explicitly proposed, was first introduced by Bevelhimer et al. [59] who performed strike tests on the Sensor Fish. Recently, Saylor et al. [66] proposed and tested flexible, fish-shaped sensor probes outfitted with accelerometers embedded in ballistic gelatin-molded bodies. However, in these studies, the relative velocity of the blade-strike was not estimated using the probe data to the knowledge of the authors.

The main contributions of this work are two-fold: **(a)** provide an open blade strike rig design, the RETERO rig, that may be used as a standardized testing and comparison environment for blade strikes on sensor probes and live fish alike, and **(b)** evaluate the suitability of the 95 g acceleration magnitude threshold as an indicator of blade strike severity using sensor probes.

The major findings of this work can be used to collect biological threshold data required to estimate injury and mortality caused by blade strikes, aid in the development of new fish-safe turbine designs, and increase the predictive accuracy of sensor probes to provide biologists and engineers with a more physically accurate representation of the frequency and severity of blade strike events in hydropower plants world-wide.

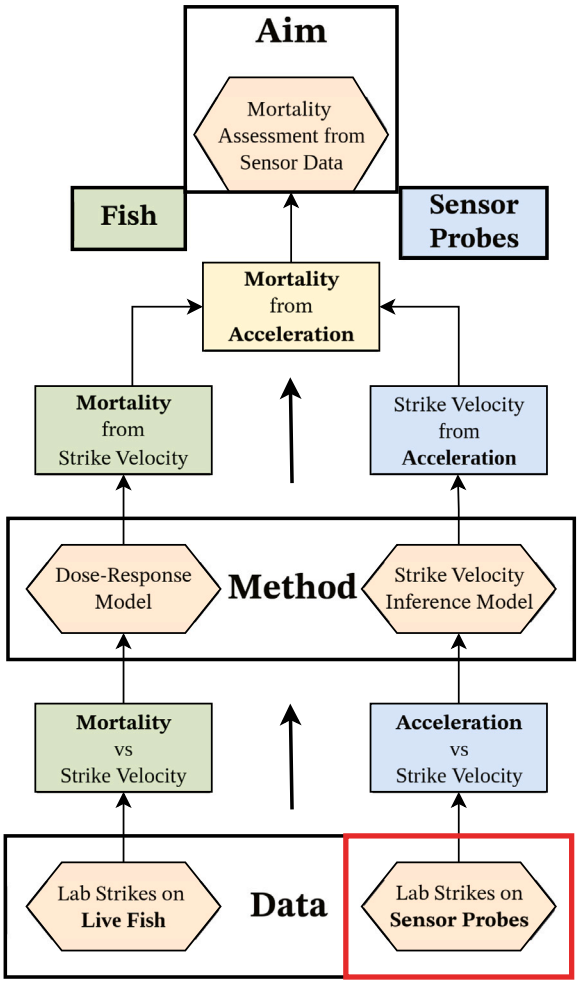

Fig. 1. Flow diagram illustrating the methodology for inferring fish mortality from sensor probe data by integrating dose–response studies with a strike velocity inference model. The sensor's acceleration time series is connected to fish mortality via the mediating variable of strike velocity. To enable this inference, data from blade strikes with known velocities (highlighted in red) is required, the means and methodology of generating these represents the primary contribution of this work.

Methodology

In this section, we compare the different strike rig designs, outline the requirements for a new strike rig, describe the proposed system, and provide a strike test protocol.

Drive system comparison. All strike rigs consist of a single turbine blade model accelerated within a static water tank. The primary objective of the rig is not to fully replicate all aspects of the hydraulic conditions within a turbine, but instead to offer a controlled testing environment that consistently generates reproducible blade strikes, facilitating the development of reliable dose–response relationships. We assessed the main difference in the existing strike rigs to be the drive system, which are electric motor-driven or spring loaded. The rig from Turnpenny et al. [57] was excluded in our study due to the difficulty in obtaining detailed information on their design, as well as the rig from Meng et al. [62] because the manuscript lacked sufficient detailed comparative design and performance data. Although spring-loaded design allows for a more compact and purely mechanical setup, the strike speed cannot be set directly. Rather, the spring tension needs to be adjusted iteratively by checking the realized strike velocity and manually changing the tension according to Bevelhimer et al. [59]. This has to be done for each velocity and blade type as the drag and probably also the inertia

of the blade changes. Furthermore, the researchers faced the challenge of a minimum spring tension that still resulted in excessive velocities, which was solved by attaching drag-increasing fixtures to the blade arm for low velocities [63]. A spring-loaded strike arm is also not able to maintain a stable velocity of the blade after collision, which can result in a significant decrease in the post-collision blade velocity. This strike characteristic differs from in-situ turbine blade collisions where the blade inertia is commonly very high. The motorized system at Alden Laboratory was therefore not faced with these challenges. The rig incorporated an additional clutch and brake system. Although the original rationale for increasing the complexity with these components was not explicitly stated, it can be inferred that their inclusion reduced the required distances for acceleration and deceleration, thus allowing for a shorter basin length. As the motor did not provide feedback, the researchers used a magnetic sensor to measure the strike velocity. As in the spring-loaded version, a stable post-strike blade velocity could not be maintained due to the lack of a closed-loop drive control. The Alden rig is considerably larger than the ORNL rig with 16.5 m versus 0.9 m, although this could potentially have been reduced by using a more powerful motor.

System requirements. We identified a number of design requirements that are necessary to ensure comparability between sensor strike experiments and live fish strike tests. However, despite differences in their underlying mechanisms, the results from both methodologies demonstrated remarkable consistency within overlapping ranges of strike velocities and fish-length-to-blade-thickness (L/t) ratios, as detailed in Section "Design challenges". We first chose the database compiled by Saylor et al. [65] which contains approximately 2300 strike tests and 250 controls which were not subjected to a blade strike [65]. We determined the fish retainer, the blade shape and the velocity range and the repeatability of the strike velocity, which need to be made as closely as possible as the retainer used in the live fish tests. The retainer applies just enough force to secure the fish or sensor probe in place while minimizing resistance to movement during strike. It also reduces variability in the input conditions but intentionally does not eliminate it entirely, as illustrated in Fig. 2. The shape of the blade had a semicircular leading edge, as introduced by Hecker et al. [64] and adopted in all ORNL rig experiments. The strike velocities of the ORNL rig range between 6.1–8.2 $m\,s^{-1}$ with a 52 mm blade and have a coefficient of variation (CV) of maximum 4% of the strike velocity. In addition, it should be safe to operate even in periods of inattention, which might arise during the hundreds or thousands of tests performed, which consist of highly repetitive tasks and can lead to a potentially higher risk of human error. We strongly encourage the development of a highly elaborated security concept for this device in case of planned copy built. Although the authors provide a detailed description of the measures taken in their lab, they cannot assume responsibility for any damage or harm in other laboratories.

Design implementation. From this point forward, the developed strike rig will be referred to as the *RETERO rig*, named after the research project within which it was developed. Fig. 2 provides an overview of the RETERO rig, illustrating the overall setup in the center. The top section details the drivetrain, featuring the linear motion system, while the bottom section depicts the sensor probe retaining system prior to a strike. The novelty of the proposed strike rig is its software configurable strike velocity, and the capacity to maintain a stable blade velocity before, during and after the impact occurs. The standoff distance of about 1 m between the basin and the ground accounts for the use of lenses with standard focal lengths in the high-speed measurement. We based our design on the motor-powered Alden rig, but improved on it by utilizing modern electronic hardware; most importantly, by using a servo drive with closed loop control. Due to its excellent starting torque and the ability to exert high breaking force, the need for an external clutch and break system is eliminated. In its software, a position control algorithm allows for setting up velocity profiles which are controlled

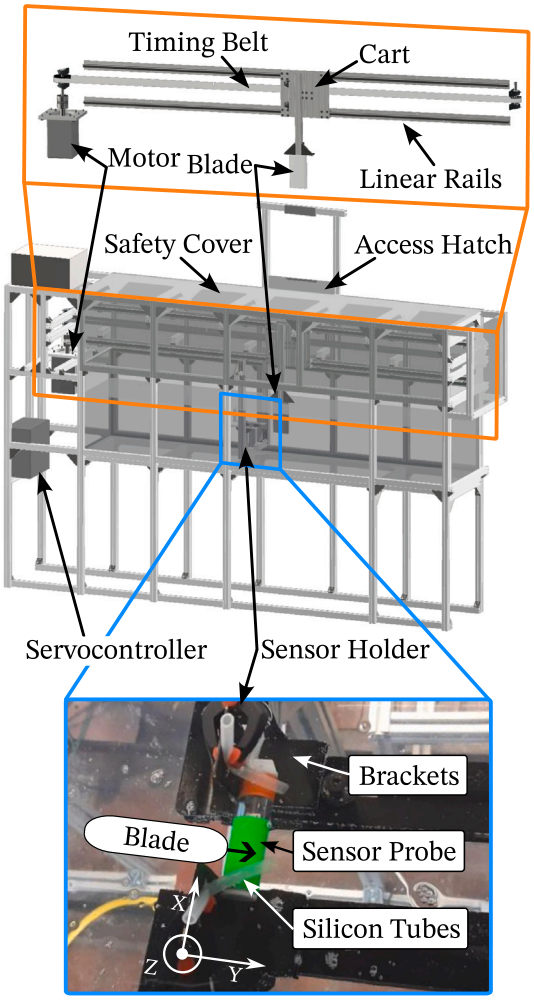

Fig. 2. Overview of the strike rig setup, with key components labeled. During operation, the blade travels linearly from left to right, striking the sensor probe positioned in the sensor holder. To minimize drag and splashing, only the blade is submerged. At the end of its travel, the blade decelerates to a predefined stop position, controlled by the servocontroller software. For safe operation, all moving parts are enclosed within acrylic glass, with an access hatch provided for sensor probe placement and retrieval. The complete setup measures 3.84 m × 0.72 m × 2.61 m (length × width × height), while the basin alone is 3.04 m × 0.582 m × 0.69 m. Below a labeled photograph showing the sensor probe positioning prior to a strike. Along the X-axis, rotation is not constrained and lateral variation in the positioning is permitted. The sensor probe is secured before impact using silicon tubes, which apply minimal force during the strike. The brackets holding the probe are 50 mm wide and 99 mm high, with a 60 mm gap between them.

and maintained using an encoder from the motor as position feedback which is fed into a closed control loop. This makes it possible to directly set the desired strike velocity by the software, without the need to iteratively find the right configuration. Additionally, through the closed loop control system, it is able to achieve a high degree of repeatability in between strikes, either performed consecutively or with intervals of days or months in between. During blade setup, the maximum achievable acceleration value must be determined, followed by fine-tuning the feedback control loops to the highest stiffness setting without inducing oscillation. This was accomplished using the 'Slider Tuning' feature in the servocontrol software (Kollmorgen Workbench), which provided more effective results compared to the 'Autotune' feature. Finally, it actively compensates for the loss of the post strike blade velocity during the strike event, which cannot be achieved with Alden or the ORNL systems as they lack the feedback for a controller. This mimics a much higher blade inertia, which is closer to reality, while

Table 1
Summary of the technical characteristics of blade strike rigs used to evaluate the risk of injury and mortality during hydropower turbine passage. The coefficient of variation (CV) for the Alden Lab rig is an own calculation based on experiment ID 21, identified as the case with maximum variance in the published data.

	Alden [58]	ORNL [59,63]	RETERO
Length × Width × Height	16.5 m × 0.91 m × 0.91 m	0.9 m × 0.6 m × 0.6 m	3.84 m × 0.72 m × 2.61 m
Drive chain	AC motor	Mechanical spring	Servomotor
Blade motion	Linear	Circle segment	Linear
Blade speed @ Blade diameter	0–12 m s^{-1} @ 150 mm	7.3–12.2 m s^{-1} @ 26 mm 6.1–8.2 m s^{-1} @ 52 mm	0–9 m s^{-1} @ 26 mm
Strike speed estimation	Automatic (Magnetic sensors)	Manual (Motion tracking)	Automatic (Motor feedback)
Repeatability as CV	**max. 1.8%**	**max. 4%**	**max. 0.12%**
Control over fish orientation & Strike angle	No	Yes	Yes
Additional features	External brake delivers high breaking force	No electronic actuation required	High-res position feedback and blade deceleration compensation

the high resolution position feedback of the motor is able to precisely quantify this effect.

The deceleration phase poses the highest risk of damage to the device itself or injury to the operators during its use, as the stored momentum of the blade must be safely dissipated. To mitigate potential damage in case of malfunction, three security measures are in place: software control ensures the blade stops near the end of its range; a limit switch positioned beyond this point cuts power to the motor; and stiff foam blocks at either end absorb the impact, preventing the cart from striking the frame or the blade from hitting the basin walls. Despite the aforementioned improvements, the RETERO rig remains affordable at 7000 € (see full cost breakdown in the appendix, Table A.3). However, even though the dimensions are more compact compared to the Alden rig, with 4.1 m × 0.7 m × 2.3 m, it is not as compact as the ORNL design.

Test protocol. The RETERO rig test protocol involved either placing the sensor probe in the holder and activating it there, or turning it on outside the water and then inserting it into the holder after verifying it was active. Sensor probes were activated using an external magnet, which when placed next to the housing in the vicinity of the magnetic switch, activated the sensor probe. The sensor probes were positioned laterally onto the strut profile and held in place using two silicone tubes, so that the blade would strike the middle of the body as shown in Fig. 2. As the effective impact stiffness of the sensor probe depends on the orientation of the printed circuit board (PCB) relative to the blade strike location, the PCB orientation was randomly set for each strike event. This is necessary to avoid a systematic bias in the accelerometer readings due to a fixed PCB orientation when the sensor probe is struck. This is an important aspect to consider when conducting strike tests in a lab because in field studies, it is not possible to ascertain the absolute orientation of the sensor probe PCB relative to the blade. By randomizing the orientation, the lab impact data are as cross-comparable with field data as possible. The longitudinal strike location within the water tank was determined and confirmed for each strike event using motor feedback to verify that the sensor probes were struck at the same position along the blade's path of motion. Sensor data quality was evaluated for further processing, to remove outliers that were indicated by acceleration magnitudes outside the measurement range or faulty recordings. Data were excluded from the strike evaluation if the acceleration magnitude peak fell outside of three times the median absolute deviation (MAD) from the median at that strike velocity, in accordance with the recommendations of Leys et al. [67,68]. The MAD is defined as: $\mathrm{MAD} = \mathrm{median}(|x_i - \mathrm{median}(X_{sv})|)$ where X_{sv} is the array of all acceleration magnitude peak values at one strike velocity and x_i is the peak value from a single experiment at that velocity, hence every strike velocity produces a different threshold.

The water level was maintained at 160 mm above the brackets on which the sensor probe is positioned prior to a strike, illustrated in Fig. 2. The blade was carefully aligned vertically during attachment, as any slant would impart a vertical velocity to the sensor probe, potentially causing it to forcefully hit the bottom of the basin or become airborne.

After reviewing the high-speed video recordings, with exemplary cases provided in the supplementary material, we conservatively set the window in which a strike occurs to 20 cm of the blade travel length. Consequently, the maximum achievable strike velocity is defined as the velocity the rig can sustain during this interval, with the same or lower velocity deviation as the rig used by Bevelhimer et al. [63], who measured the blade velocity immediately before impact. We refer to this as the minimum strike window requirement (MSWR), set at 20 cm.

Data processing. To combine and process data from the sensor probes, servocontroller, and high-speed video, a series of Python scripts have been developed and made openly available.[1] These scripts are bundled into a Python package, which can be installed easily via the Python package manager pip. The overall workflow, illustrated in the Github repository, begins by importing the data and checking for corruption or outliers caused by technical faults or operator errors, as described in the above paragraph.

The dataset is trimmed to the strike event by identifying the first collision point where the acceleration magnitude reaches the dynamically adjusted threshold determined in accordance to [68]. This value is also used to verify data integrity, and then including an additional 4 ms prior to this point to ensure no relevant information is lost.

The processed data is then organized along three dimensions: strike velocity, trial, and time, using the Xarray Python package.[2]

RETERO rig repeatability

High repeatability between strikes is achieved through a 4 kHz closed-loop feedback control system between the servocontroller and motor. To assess the rig's repeatability, we conducted tests without a sensor probe, measuring the strike velocity at the impact position for velocities between 1 m s^{-1} to 10 m s^{-1}, with five repetitions per velocity. The coefficient of variation (CV), used as a repeatability metric by Bevelhimer et al. (see Table 1), was 0.12 % at 1 m s^{-1} in our rig, significantly lower than their reported 4%. Achieving high precision is crucial, as we aim for equal or better repeatability to ensure reliable comparison with previous strike rig study results. Additional metrics for each strike velocity can be found in Table 2.

Results & discussion

To illustrate the trajectory of the strike blade at velocities ranging from 1 m s^{-1} to 10 m s^{-1}, Fig. 3 presents the corresponding velocity

[1] github.com/ikoesters/srdatacombiner.
[2] docs.xarray.dev.

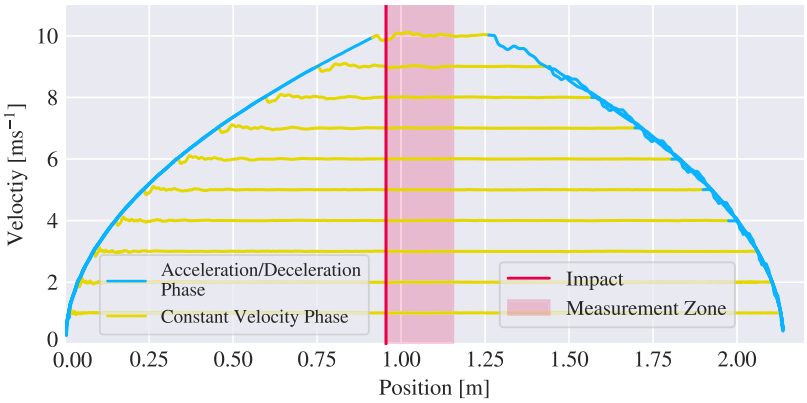

Fig. 3. Blade velocity trajectories from 1–10 m s^{-1} without strike events over the whole range of motion of the system. These trajectories represent standard trapezoidal velocity profiles in the time domain. The trapezoid shape is determined by the stop position, the acceleration and deceleration, and the velocity, which are manually set during the motor configuration. Gain factors for the control loop are automatically determined during startup.

Table 2
Overview of the various metrics assessing precision and repeatability across target strike velocities ranging from 1 m s^{-1} to 10 m s^{-1} at 0.955 m along the path of travel of the blade. The coefficient of variation (CV) is equivalent to the relative standard deviation, the median absolute deviation (MAD) was normalized by the strike velocity as well.

Target velocity [m s^{-1}]	Mean [m s^{-1}]	CV [%]	Median [m s^{-1}]	Rel. MAD [%]
1	1.00	**0.12**	1.00	**0.05**
2	2.00	0.02	2.00	0.01
3	3.00	0.05	3.00	0.03
4	4.00	0.03	4.00	0.01
5	5.01	0.02	5.00	0.02
6	6.00	0.01	6.00	0.01
7	7.00	0.02	7.00	0.02
8	8.01	0.03	8.01	0.02
9	8.98	0.01	8.98	0.00
10	9.89	0.02	9.89	0.01

profiles over the strike path without collision. Initially, the blade accelerates with 55 m s^{-2} (0–10 m s^{-1} in 0.18 s) to the target velocity, maintaining it as consistently as possible despite any disturbances. With a 9.5 mm blade, mechanical losses and drag losses combined use between 4% (1 m s^{-1}) and 13%(10 m s^{-1}) of the available 30 A power budget, with the remaining power used to overcome the inertia of the system. These values were calculated on the constant velocity part of corresponding trajectories without strikes between 1–8 m s^{-1} with a coefficient of determination of $r^2 = 0.990$. At the moment of impact, a brief deceleration occurs, which is promptly counteracted by the servocontroller, increasing the motor power to restore the target velocity. The velocity loss during the strike was calculated as the difference between the target strike velocity and the minimum velocity observed during the strike, ranging from 3.1–5.3 % of the strike velocity measured directly before impact. Finally, the blade decelerates with 57 m s^{-2} and comes to a complete stop at a predefined location. To investigate performance during strike tests with large and heavy sensor probes, a trout model (33 cm in length, 620 g) was constructed as described in [69]. The model is built from a 0.2 mm carbon fiber composite sheet as a mid-plane, a body made of two-component silicone (Zhermack Elite Double 8), and a stiff 3D-printed head.

Example use-case

To showcase a practical application of the strike rig we performed strike tests on sensor probes. The investigation aims to shed light on the challenges associated with the use of an acceleration magnitude threshold to assess the severity of a strike event. In this investigation, the sensor probe was subjected to blade strikes of 1 m s^{-1} with 30 repetitions each. The position of the sensor probe before the strike was controlled as shown in Fig. 2. The blade featured a semicircular leading edge with a 9.5 mm diameter, made from 3D-printed impact-resistant polycarbonate (PC) and reinforced by stainless steel threaded rods. The sensor probe used is the Robust Autonomous Pressure and Inertial Device (RAPID), developed at the Tallinn University of Technology and are certified for impacts according to the M802:01.03.2022 shock test procedure (peak accelerations from 10–400 g) and ECSS-E-ST.10-03C(2012) test standard with the test certificate nr. 8-009-22/13.04.2022. It is neutrally buoyant, 25 mm in diameter, 100 mm long, and has a mass of 24 g, which are similar dimensions to those of the Sensor Fish of Deng et al. [36], and records the acceleration in three axes over a range of 400 g at a rate of 2 kHz. The time of peak acceleration magnitude varies across four measurement points, or approximately 1.5 ms, with a median strike duration of 3 ms, considering values above 10 g. Following the convention of Deng et al. [38], where values within 70% of the peak are counted, the strike duration ranges between 0.5–1 ms (1–2 data points). Additionally, not all time series exhibited a single distinct peak; many showed two peaks, separated by a data point significantly lower than the adjacent values.

Fig. 5 presents the results of our experiment, in which strikes at 1 m s^{-1} produced a mean acceleration peak of 200 g, well above the 95 g threshold, though still within the 7.5 ms time window used to classify a strike event [38]. A left-tailed 95% confidence interval, calculated using the Student's t-distribution to determine the margin of error, provides a lower bound of 184 g. Strikes exceeding this threshold have been associated with severe injuries according to [38]. However, the database compiled by Bevelhimer et al. [63], which includes over 2500 live fish blade strike tests of a variety of fish species, reports minimal mortality even at velocities of 5 m s^{-1}, with only one fatality out of 55 fish tested. In the comprehensive overview study by Pflugrath et al. [70], an extended model based on strike tests involving seven different fish species with varying mean body sizes (*Alosa* spp.: 7.6 cm; Gizzard shad: 16 cm; Paddlefish: 26.7 cm; Rainbow trout: 11.6 cm and 16.1 cm; Hybrid striped bass: 18 cm; Bluegill: 11.6 cm and 16.1 cm; Brook trout: 24.8 cm) resulted in dose–response curves predicting zero mortality for strike velocities below 5 m s^{-1} across all tested species and sizes. This suggests that while the 95 g criterion has been a valuable guideline, its reliability as a predictor of mortality, already being subjected to increasing scrutiny regarding its accuracy [53], is not likely that it is a reliable threshold to evaluate mortality from simulated turbine strikes. This is further supported by Bevelhimer et al. [59] which noted that the maximum accelerations observed in their strike apparatus were higher than those reported in field studies of that period using the Sensor Fish device. This leads to the authors hypothesis that this overestimation is a systematic problem and not related to the specific sensor technology used in this study as it appears in both sensor probe designs, using two different strike rigs by independent investigators. Consequently, further refinement of a strike parameter on sensor probes is necessary to more reliably infer blade strike velocity from acceleration measurements.

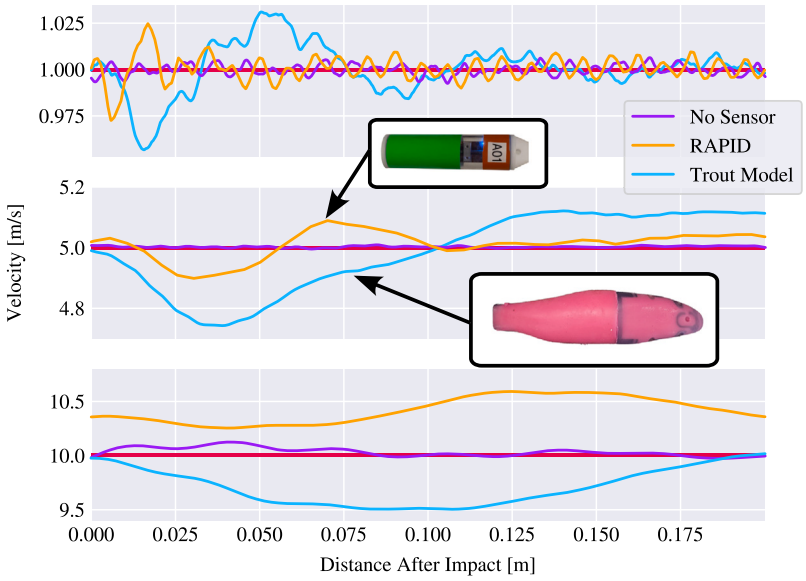

Fig. 4. Average blade speed, measured by the servocontroller in relation to its position post-impact, was recorded for cases with no sensor, the RAPID sensor (described in the following example use-case), and the trout model at strike velocities of $1\,m\,s^{-1}$, $5\,m\,s^{-1}$, and $10\,m\,s^{-1}$ (indicated by the red bar) struck mid-body, laterally. At $5\,m\,s^{-1}$, it can be observed that, despite the substantial weight and size differences between the RAPID sensor (24 g, 90 mm) and the trout model (620 g, 330 mm), the additional reduction in strike velocity due to drag and impulse transfer for the trout model is only $0.16\,m\,s^{-1}$. At $10\,m\,s^{-1}$, the trout model exhibited a maximum deceleration of $0.5\,m\,s^{-1}$, compared to $0.05\,m\,s^{-1}$ for the RAPID sensor. A systematic error of $0.3\,m\,s^{-1}$ or 3% in the realized strike velocity can be observed in the RAPID sensor measurements due to an improper servocontroller configuration, however, it was deemed negligible to the overall results considering the variation in measured acceleration, shown in the subsequent Section "Example use-case".

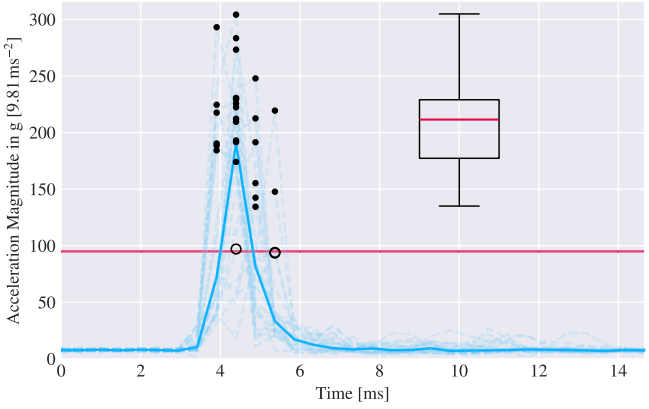

Fig. 5. Acceleration time series for strikes at $1\,m\,s^{-1}$ are shown as transparent dashed blue lines ($n = 30$), with the median acceleration represented by a solid blue line. Black dots indicate peak acceleration values for each time series, where it can be seen that all acceleration magnitudes exceeded the 95 g threshold at $1\,m\,s^{-1}$. The distribution of peak values is represented in the box-whisker plot on the right, with whiskers extending to 1.5 times the interquartile range and outliers indicated by empty circles. The median peak acceleration is 211 g, with one strike reaching 304 g. In all but one trial the 95 g threshold was exceeded, highlighted by the horizontal red line. The post-impact acceleration is caused by the blade's wake.

Design challenges

Several challenges were identified during the development and operation of the RETERO rig. These include limitations related to maximum velocity, motor interaction, and structural stability, which are detailed below. The differences between the turbine environment and the strike rig do not necessarily constitute a limitation. Rather, the rig was deliberately designed not to replicate the precise physical conditions of turbine passage, but instead to simulate blade strikes in the controlled and reproducible manner of a lab environment while minimizing confounding factors.

Maximum velocity. Although the ORNL strike rig is capable of achieving velocities up to $12.2\,m\,s^{-1}$, our current design is limited to a maximum strike velocity of $10\,m\,s^{-1}$. This constraint arises from the minimum strike window requirement (MSWR) of 20 cm, set in our test protocol. Achieving higher velocities would reduce the strike window below this threshold. Nonetheless, this limitation might be not of major concern, as average mortalitiy rates provided in dose–response studies reported very high to total mortality risks already below 10 m/s for many species and live stages such as shown by [65] for small (11–12.5 cm) and larger (22–26 cm) rainbow trout. If higher impact speeds became necessary for a specific experimental campaign, a more powerful servo controller and motor would be required to deliver additional power. Beside this reducing the accelerated mass is another potential strategy to lower power demands. A script for evaluating these scenarios, calibrated using real-world data from our rig, is available in the code repository.

Stability. To prevent excessive vibration during operation, which increases with strike velocity and blade thickness, the rig should be supported by a stable foundation which is an important consideration when selecting the location for the RETERO rig. Ideally, this support should also be provided at the top of the rig for maximum leverage.

Additionally, we recommend that the high-speed camera setup be mounted separately from the rig's frame to prevent interference. Even though shaking cannot be completely eliminated, image sharpness was not adversely affected by post-strike vibrations in our tests, suggesting that most of the vibrations occurs after the strike.

Comparability rotary motion and linear motion strikes. The design of the linear motion strike rig is based on the assumption that tangential motion during impact is a reasonable approximation for impacts in rotary machines. While this may hold true for hard-bodied sensor probes, where the strike may be characterized primarily by the initial impact, soft-bodied objects, such as fish or soft-bodied sensor probes, can experience significantly longer interactions with the blade. In the worst-case scenario, where the interaction spans the entire strike window of 20 cm, the angular rotation is given by $\Phi = \frac{2s_{\text{travel}}}{d_{\text{rotor}}}$, where s_{travel} is the 20 cm strike window and d_{rotor} is the rotor diameter. The resulting deviation perpendicular to the strike direction is given by $x_{\text{deviation}} = (1 - \cos(\Phi)) \cdot s_{\text{travel}}$. For typical machine dimensions, such as a turbine with a 8.6 m rotor [42] and a pump with a 0.8 m [32] rotor, this deviation ranges from 0.22 mm for the turbine to 24 mm for the pump or 0.1 % and 12.2 % in relation to the travel length respectively. According to Bevelhimer et al. [59], the blade swept through 0.5 m of water before impact. Assuming an approximate angular rotation of 90°, this corresponds to an estimated rotor with a 0.64 m diameter with a resulting geometric deviation of 40 mm (or 19%) when compared to linear motion.

Additionally, we compared compiled results from live fish strike tests on rainbow trout (*Oncorhynchus mykiss*) conducted by Electric Power Research Institute (EPRI) [58] and ORNL [65] for overlapping values of the L/t ratio and strike velocity. While ORNL reported data for individual strikes, EPRI provided averaged results, leading to a comparative approach where EPRI datasets encompassing similar experimental conditions to ORNL were included, as illustrated in Fig. 6(b). Both studies used a blade with a semicircular leading edge and assessed mortality at 1 h post-strike. ORNL reported fish length as total length (from the tip of the snout to the tips of the caudal fin), while EPRI reported fork length (measured from the tip of the snout to the middle caudal fin rays) [64]. This methodological difference is expected to have minimal impact for rainbow trout, as this species has relatively short fin tips, resulting in a nearly truncate caudal fin. EPRI's experiments varied strike location, primarily targeting the mid-body, and did not control for fish orientation, though both parameters were documented. In contrast, ORNL's selected strikes had a consistent lateral orientation but varied in strike location, with box 3 in Fig. 6(b) consisting entirely of strikes to the tail region, which is summarized in Fig. 6(a). Despite methodological differences, mortality discrepancies across the three overlapping cases were minimal, showing that the rigs with linear motion show good comparability to those with rotary motion.

Deviation of the impact location. In Fig. 4, it can be observed that the impact position shifts towards the rear between strike velocities of $1\,\text{m}\,\text{s}^{-1}$ to $10\,\text{m}\,\text{s}^{-1}$ by 10 cm. In Table 2, we assumed a constant impact position, corresponding to the impact location for a strike velocity of $1\,\text{m}\,\text{s}^{-1}$. This assumption introduces inaccuracies at higher velocities, as the impact occurs later than expected. However, given the high repeatability of the strike event and the significant variability in the measured acceleration magnitude of the sensor probe following the strike, correcting for this rather small positional error was deemed to have little meaningful impact on the measurements.

Conclusions & Outlook

Hydropower is a vital component of global renewable energy strategies. However, its ecological challenges, in particular the risk of injury and mortality to fish during downstream passage, pose an obstacle for a continued use in the face of the increased awareness of its ecological impact and the loss of biodiversity. The test rig presented in this work bridges a critical gap in hydropower research by offering a reproducible platform for studying the dynamics of blade strikes on sensor probes and live fish data. In this work, we introduced a digitally controlled, open-access laboratory test rig design for the collection of biological threshold data necessary for estimating fish injury and mortality due to turbine blade strikes, with detailed design information available online [71]. The rig also allows for an enhancement of the predictive accuracy of passive collision sensors, providing biologists and engineers with a more accurate depiction of the frequency and severity of blade strike events. This tool is especially valuable for developing new fish-safe turbine designs, because it allows for impact testing multiple blade geometries across a range of strike velocities. With precise control over blade velocity, ranging from $1\,\text{m}\,\text{s}^{-1}$ to $10\,\text{m}\,\text{s}^{-1}$, it offers a reliable method for studying both fish injury and the physical conditions experienced during strikes. The open-access design significantly lowers the barrier to entry by reducing the need for specialized engineering expertise, making it more accessible to researchers from various fields.

Existing laboratory methods to research strike events, such as live fish experiments and sensor-based testing, have been constrained by the lack of precise control over blade velocity and the absence of a standardized test rig. Our rig addresses these limitations with electronically controlled blade velocity, improved reproducibility between strikes, minimal and quantified deceleration during impact, self-resetting mechanisms, and high-resolution position feedback—all within a compact and cost-efficient design. The fact that even strikes at $1\,\text{m}\,\text{s}^{-1}$, which are insufficient to cause severe injury to fish, produced acceleration values exceeding the 95 g threshold by more than double, not only challenges the current reliance on this threshold for determining injury severity but more importantly shows the need of improved sensor development and the benefit of having access to a system like ours, which allows researchers to verify blade strike models under controlled conditions. This setup isolates strike events from other confounding effects of a real flow field, focusing exclusively on strike velocity and blade thickness which are two critical variables influencing mortality to provide data specifically suited for estimating strike severity in field conditions using sensor probes. This approach could significantly enhance ecological impact assessments of hydropower facilities by enabling the use of dose–response relationships to estimate strike-induced mortality for specific fish species solely from sensor data — an application not currently feasible in field investigations. Current live fish testing methods, involving extensive fieldwork and intensive data processing, are highly time-consuming and challenging to scale. For instance, one of the authors participated in a recent live-fish experiment involving over 1800 fish, combined with sensor probes, to investigate changes in passage mortality for three fish species in a pump modified specifically to reduce fish mortality [72]. This study required several weeks of fieldwork followed by more than nine months of data cleaning and analysis.

Looking ahead, the development and use of this test rig offer new opportunities to refine injury and mortality models based on sensor data as well as aid in advances of sensor development regarding the prediction of strike velocity. Future work could focus on expanding the rig's capabilities to test a broader range of conditions and sensor types. Additionally, the open design allows for collaboration within the hydropower, engineering, and biological communities to further enhance the predictive models used in assessing fish injury and mortality. By refining sensor probe accuracy, the need for live fish testing in field studies can be reduced, promoting more ethical and efficient research methods. Ultimately, the continued evolution of such test rigs will contribute to more sustainable and ecologically responsible hydropower development worldwide.

	Strike Velocity [m/s]	L/t Ratio [-]	Amaral et al. n	Amaral et al. Loc [%]	Amaral et al. Orient [%]	Amaral et al. Survival [%]	Bevelhimer et al. n	Bevelhimer et al. Loc [%]	Bevelhimer et al. Orient [%]	Bevelhimer et al. Survival [%]	**Discrepancy [%pt.]**
Box 1	7.8–8.6 (8.1)	2.0–2.7 (2.3)	50	4 H 74 M 22 T	64 L 22 D 14 V	32.0	20	10 H 90 M 0 T	100 L 0 D 0 V	30.0	**2.0**
Box 2	7.0–7.4 (7.2)	1.6–2.7 (2.2)	50	21 H 65 M 15 T	65 L 25 D 10 V	78.0	20	0 H 95 M 5 T	100 L 0 D 0 V	75.0	**3.0**
Box 3	7.9–8.3 (8.1)	1.0–1.5 (1.2)	14	0 H 71 M 29 T	93 L 0 D 7 V	92.9	16	0 H 0 M 100 T	100 L 0 D 0 V	93.8	**0.9**

(a) Table comparing experiments with overlapping conditions identified in fig. 6b, with the mean values reported by Amaral et al. in brackets. Strike location, reported as head (H), mid-body (M), and tail (T), and fish orientation, as lateral (L), dorsal (D), and ventral (V).

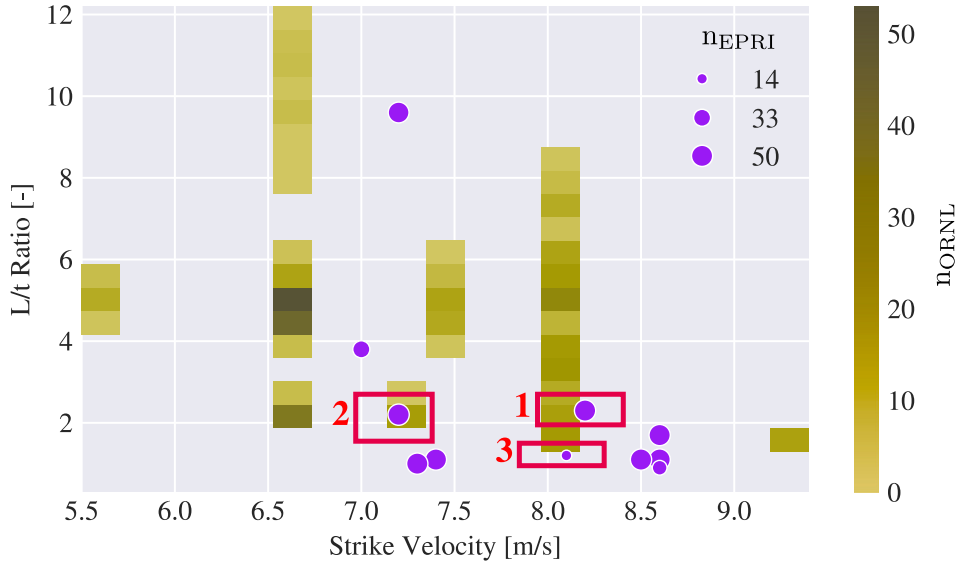

(b) Strike experiments conducted at EPRI as purple circles, and ORNL shown in yellow, with overlapping experiments within the red boxes.

Fig. 6. Comparison of strike experiments on rainbow trout between the ORNL and EPRI experiments, with three identified overlapping conditions. ORNL results, reported individually, are represented as a yellow heat map, while EPRI's averaged results are shown as purple circles. For comparing L/t ratios (ratio of fish length to blade thickness), the minimum and maximum values reported from EPRI for that experiment were used, while a 5% range around the reported strike velocity was applied to identify overlapping conditions. Despite notable variations in strike location and fish orientation (as shown in the table), the discrepancy in reported mortality rates remains minimal.

CRediT authorship contribution statement

Wolf Iring Kösters: Writing – original draft, Visualization, Validation, Software, Methodology, Investigation, Data curation. **Jeffrey A. Tuhtan:** Writing – review & editing, Validation, Supervision, Methodology, Conceptualization. **Danil Efimov:** Investigation. **Maarja Kruusmaa:** Writing – review & editing, Supervision, Resources, Project administration, Funding acquisition. **Stefan Hoerner:** Writing – review & editing, Validation, Supervision, Resources, Project administration, Methodology, Funding acquisition, Conceptualization.

Declaration of competing interest

The authors declare that they have no known competing financial interests or personal relationships that could have appeared to influence the work reported in this paper.

Acknowledgments

The authors would like to express their sincere gratitude to Karla Ruiz-Hussmann, Jessica Dafis, Yanneck Kiiski, Shokoofeh Abbaszadeh, Christian Kisow, and Dirk Meinecke for their invaluable assistance in the construction of the strike rig. Special thanks are extended to Yanneck Kiiski and Johannes Frank for their contributions to the creation and maintenance of the CAD design. Finally, we are deeply appreciative of Roberto Leidhold for his crucial support in the setup and tuning of the power electronics and servomotor, without which this project would not have been possible.

This project is part of the EU Marie Curie International Training Network on Soft, Self-responsive, Smart Materials for Robots (SMART-ITN) and has received funding from the European Union's Horizon 2020 research and innovation program under the Marie Sklodowska-Curie grant agreement No 860108. It is also funded by the German Federal Ministry of Education and Research (BMBF) under project number 031L0152A - D/16LW019 ("Alternative Methods to Animal Testing"), which ran between March 2019 to March 2024 and received funding by the Deutsche Forschungsgemeinschaft (DFG, German Research Foundation), Germany – 444994527. Jeffrey A. Tuhtan and Maarja Kruusmaa's contributions were funded in part by the Estonian Research Council, Estonia Grant PRG2198.

Appendix A. Detailed design description

Detailed instructions for constructing the strike rig are provided in this section. Table A.3 shows a cost breakdown for each assembly group, while individual part names, numbers and additional info on these parts important for building the strike rig can be obtained in the bill of materials table available online [71].

Table A.3
Cost breakdown of the strike rig and its assembly components as of late 2022. Prices have remained largely stable as of 2024.

Assembly group	Main items in group	Approximate price
Frame	aluminum strut profiles, brackets, fasteners	1800 €
Basin	PC plates, PU adhesive, primer	1200 €
Drive system mechanics	rail, belt, linear bearings, pulleys, bushings	900 €
Drive system electronics	motor, servo-drive, break resistor	3100 €
	Total	**7000 €**

The strike rig is a linear motion system with supported rail, as this combines high stiffness and load capacity with low cost. The drive system is a servo-motor, it allows for high-accuracy motion control and the ability to engage with the maximum torque from rest. The torque is transmitted through a timing belt; this is much lighter and does not need lubrication compared to a chain. The frame is comprised of aluminum strut profiles 45 mm × 45 mm in size that allow easy modification and construction while being decently stiff.

The strike rig employs a linear motion system with supported rails, offering a combination of high stiffness, load capacity, and cost-efficiency. The drive system consists of a servo motor, providing high-accuracy motion control and the capability to deliver maximum torque from rest. Torque is transmitted via a timing belt, which is lighter and requires no lubrication compared to a chain. The frame is constructed from 45 mm × 45 mm aluminum strut profiles, ensuring ease of modification and assembly while maintaining sufficient stiffness.

To estimate the required motor power, the motion system was initially modeled using differential equations that accounted for mass, acceleration, and fluid drag. Following the rig's construction, these values were updated to include real-world mechanical losses. For research groups interested in building a similar system, the Python script used for these calculations is available in the GitHub repository.[3]

Frame and basin. The basin is constructed from polycarbonate (PC) due to its superior impact resistance compared to glass or acrylic glass. Standard PC plates are produced in dimensions of 3050 mm × 3050 mm, which determined the basin length of 3 m to eliminate the need for additional seals. To address expected pressure peaks, sloshing effects, and wave-induced deformation, a flexible polyurethane adhesive (Sika Sikaflex 295UV) was used. To enhance stiffness, the PC plates were reinforced with aluminum angle profiles along their edges. The basin is supported by a frame of aluminum strut profiles, which bear the basin's load and provide mounting points for other system components.

Motor. The maximum motor speed and effective pulley diameter determine the system's maximum strike speed and should be selected to achieve the desired performance. An excessively large pulley diameter increases the required translational force, leading to higher torque demands and necessitating a more powerful motor and servo drive. The motor selected for the system is a Siemens 1FT6102-8AC71, which provides a maximum speed of 1500 RPM at full torque. This corresponds to an optimal pulley diameter of 127 mm.

Servocontroller. The servocontroller used (Kollmorgen AKD-P01207) is capable of delivering a peak current of 30 A for up to 1 s, resulting in motor power of 10.4 kW when supplied with three-phase current at 400 V. A key advantage of this controller is its compatibility with Python, enabling the development of an interface to adjust parameters within predefined safe limits. Additionally, more advanced velocity trajectories can be programmed and fed through the PC interface. During deceleration, the motor operates as a generator, with the generated energy dissipated as heat through an external resistive load.

[3] github.com/ikoesters/srdatacombiner.

Belt and pulleys. A belt drive was selected over a chain drive or spool system, as used by the Alden rig, due to its lower weight compared to a chain drive and its ability to enable automatic resetting, which is not feasible with a spool system. The HTD (high-torque drive) system was chosen for its high availability and superior circumferential force capacity. The specific belt used is an HTD-8M-30, featuring a 8 mm tooth pitch and a 30 mm width. Proper belt tension is achieved by adjusting the axial distance, moving the motor setup backward as necessary.

The pulley is not mounted directly to the motor shaft because the radial forces generated exceed the shaft's maximum allowable force. Instead, the pulley is mounted on a separate shaft connected to the motor via a backlash-free metal bellows coupler, which is critical for avoiding resonance in the system. The shaft, with a diameter of 20 mm, is made from X46Cr13 stainless steel and is supported by two UCP204 industry-standard pillow bearings. Its dimensions were determined using the von Mises yield criterion with a safety factor of 1.4.

The closest available match to the effective diameter in the HTD-8M system is a 48-tooth motor pulley, which allows for a maximum speed of 9.6 m s^{-1}. Although slightly below the desired speed of 10 m s^{-1}, the torque loss associated with this discrepancy is minimal and does not significantly affect performance.

Rail and cart. A shaft-guidance system of type TBS25, featuring 25 mm diameter shafts with a length of 3200 mm, was used. This system is compatible with the aluminum strut profile raster, ensuring seamless integration. The cart is connected to the rail through low-friction recirculating ball bearings (SBR25UU), providing smooth and efficient motion.

The cart itself is constructed from planar aluminum strut profiles, allowing for rapid attachment or replacement of the blade arms. The belt is secured to the cart using clamping plates.

Strike arm and blade. The strike arm is constructed from an aluminum strut profile, onto which 3D-printed impact-resistant polycarbonate (PC) blades are attached. The 3D-printed blades are reinforced with two stainless steel threaded rods, which are epoxied into the structure and serve as connection points to the strut profile. A plastic lid positioned between the blade and the strike arm acts as a splash shield.

To ensure comparability with the data from Saylor et al. [65], the blade's leading edge is constrained to a semicircular shape. However, the supporting body and trailing edge of the blade can be optimized to reduce drag and, more importantly, to minimize entrained air, which negatively effects high-speed video quality.

Sensor retainer. The sensor mounting setup follows the design established by ORNL [63]. Two angled aluminum sheets, each 50 mm wide, are mounted on the front side of an aluminum strut profile, as illustrated in Fig. 2. The strike angle can be adjusted by repositioning the aluminum platforms and securing them with wing nuts. The distance between the platforms is adjustable by moving the strut profile to which the platforms are attached.

Data synchronization. The servocontroller is programmed to emit a digital pulse before impact, serving as a trigger signal for the high-speed cameras. Additionally, this signal activates a device that generates a magnetic pulse via a copper coil on the basin wall adjacent to sensors that feature Hall effect sensors. This pulse is detected by a magnetic

sensor on the probe and is later used for synchronizing the data from the servo-drive, cameras, and sensor probe. For sensors without a Hall effect sensor, the sudden increase in acceleration magnitude upon impact may be used to achieve synchronization.

Safety considerations. To reiterate was has been said in the methodology section, ensuring safe operation is paramount, even in cases of user inattention. To this end, the rig is fully enclosed in acrylic glass, and the access hatch is equipped with a safety switch that disables the motor when opened. Additionally, a Python-based graphical user interface is under development to restrict access to the servocontroller software, allowing only safe and predefined user inputs.

Incorrect parameter settings in the servocontroller software can lead to potentially catastrophic outcomes, particularly concerning the end-of-motion point. This setting allows the motor to operate at full speed up to the limit switch, which cuts power if exceeded. However, the momentum stored in the system can cause the motor to crash into the wall beyond the limit switch. While buffer material has been successfully used to soften such impacts and prevent structural damage, this mitigation measure cannot be guaranteed to protect against all scenarios.

Appendix B. Supplementary data

The supplementary material [73] includes high-speed videos of the fish dummy discussed in Section 3 and the rigid RAPID sensor probe impacted at $5\,\mathrm{m\,s^{-1}}$, recorded from the bottom and side, along with a strike video at normal speed, available at https://doi.org/10.5281/zenodo.15864853.

Data availability

The CAD data are publicly available online [71], and the software used for data processing and integration can be accessed via GitHub at https://github.com/ikoesters/srdatacombiner. Videos demonstrating the RETERO strike rig tests are included in the supplementary materials. Additionally, the datasets used to generate Figures 4, 5, and 6 in this paper are openly accessible online [74].

References

[1] Vagnoni E, Gezer D, Anagnostopoulos I, Cavazzini G, Doujak E, Hočevar M, Rudolf P. The new role of sustainable hydropower in flexible energy systems and its technical evolution through innovation and digitalization. Renew Energy 2024;230:120832. http://dx.doi.org/10.1016/j.renene.2024.120832, URL https://linkinghub.elsevier.com/retrieve/pii/S0960148124009005.

[2] Cox RX, Kingsford RT, Suthers I, Felder S. Fish injury from movements across hydraulic structures: A review. Water 2023;15(10):1888. http://dx.doi.org/10.3390/w15101888, URL https://www.mdpi.com/2073-4441/15/10/1888.

[3] Iho A, Soininen N, Vehviläinen I, Koljonen S, Artell J, Belinskij A. Rivers under pressure: Interdisciplinary feasibility analysis of sustainable hydropower. Environ Policy Gov 2023;33(2):191–205. http://dx.doi.org/10.1002/eet.2013, URL https://onlinelibrary.wiley.com/doi/10.1002/eet.2013.

[4] Van Treeck R, Radinger J, Noble RA, Geiger F, Wolter C. The European fish hazard index – an assessment tool for screening hazard of hydropower plants for fish. Sustain Energy Technol Assessments 2021;43:100903. http://dx.doi.org/10.1016/j.seta.2020.100903, URL https://linkinghub.elsevier.com/retrieve/pii/S2213138820313308.

[5] Larinier M. Contributing paper dams and fish migration. In: World commission on dams. 2001, URL https://www.semanticscholar.org/paper/Contributing-Paper-Dams-and-Fish-Migration-Larinier/e4ab7319c3a47876392607a3f277fe03a64fc6b1.

[6] Błońska D, Tarkan AS, Andreou D, Bolland JD, Davies P, Dodd JR, Gillingham P, Roberts CG, Amat-Trigo F, Aksu S, Hindes A, Palder OJ, Yeldham M, Britton JR. Restoration of river connectivity enables long-distance spawning migrations in a potamodromous fish. J Environ Manag 2025;377:124646. http://dx.doi.org/10.1016/j.jenvman.2025.124646, URL https://linkinghub.elsevier.com/retrieve/pii/S030147972500622X.

[7] Union TE. Directive 2000/60/EC of the European Parliament and of the Council of 23 October 2000 establishing a framework for Community action in the field of water policy. 2000, URL https://eur-lex.europa.eu/eli/dir/2000/60/oj.

[8] Brown E, Sulaeman S, Quispe-Abad R, Müller N, Moran E. Safe passage for fish: The case for in-stream turbines. Renew Sustain Energy Rev 2023;173:113034. http://dx.doi.org/10.1016/j.rser.2022.113034, URL https://linkinghub.elsevier.com/retrieve/pii/S1364032122009157.

[9] Uria-Martinez R, Johnson M. U.S. hydropower market report (2023 edition). Technical report, Oak Ridge National Laboratory (ORNL), Oak Ridge, TN (United States); 2023, URL https://www.energy.gov/eere/water/hydropower-market-reports.

[10] Quaranta E, Aggidis G, Boes RM, Comoglio C, De Michele C, Ritesh Patro E, Georgievskaia E, Harby A, Kougias I, Muntean S, Pérez-Díaz J, Romero-Gomez P, Rosa-Clot M, Schleiss AJ, Vagnoni E, Wirth M, Pistocchi A. Assessing the energy potential of modernizing the European hydropower fleet. Energy Convers Manage 2021;246:114655. http://dx.doi.org/10.1016/j.enconman.2021.114655, URL https://linkinghub.elsevier.com/retrieve/pii/S0196890421008311.

[11] Schwevers U, Adam B. Fish-friendly turbines. In: Schwevers U, Adam B, editors. Fish protection technologies and fish ways for downstream migration. Cham: Springer International Publishing; 2020, p. 203–10. http://dx.doi.org/10.1007/978-3-030-19242-6_6.

[12] Foust J, Hecker G, Li S, Allen G. Fish-Friendly hydropower turbine development & deployment: alden turbine preliminary engineering and model testing. Technical report DOEGO18167-1, Electric Power Research Institute; 2011, http://dx.doi.org/10.2172/1050066, URL https://www.osti.gov/biblio/1050066.

[13] Quaranta E, Bahreini A, Riasi A, Revelli R. The very low head turbine for hydropower generation in existing hydraulic infrastructures: State of the art and future challenges. Sustain Energy Technol Assessments 2022;51:101924. http://dx.doi.org/10.1016/j.seta.2021.101924, URL https://www.sciencedirect.com/science/article/pii/S2213138821009383.

[14] Amaral SV, Watson SM, Schneider AD, Rackovan J, Baumgartner A. Improving survival: Injury and mortality of fish struck by blades with slanted, blunt leading edges. J Ecohydraulics 2020;5(2):175–83. http://dx.doi.org/10.1080/24705357.2020.1768166, URL https://www.tandfonline.com/doi/full/10.1080/24705357.2020.1768166.

[15] Klopries E-M, Deng ZD, Lachmann TU, Schüttrumpf H, Trumbo BA. Surface bypass as a means of protecting downstream-migrating fish: Lack of standardised evaluation criteria complicates evaluation of efficacy. Mar Freshwater Res 2018;69(12):1882–93. http://dx.doi.org/10.1071/MF18097, Publisher: CSIRO PUBLISHING. URL https://www.publish.csiro.au/mf/MF18097.

[16] Knott J, Mueller M, Pander J, Geist J. Downstream fish passage at small-scale hydropower plants: Turbine or bypass? Front Environ Sci 2023;11:1168473. http://dx.doi.org/10.3389/fenvs.2023.1168473, URL https://www.frontiersin.org/articles/10.3389/fenvs.2023.1168473/full.

[17] Norman J, Reeds J, Wright RM, Bolland JD. Impact of anthropogenic infrastructure on aquatic and avian predator–prey interactions in a modified lowland river. Freshwater Biol 2024;69(1):157–71. http://dx.doi.org/10.1111/fwb.14201, URL https://onlinelibrary.wiley.com/doi/10.1111/fwb.14201.

[18] Radinger J, Van Treeck R, Wolter C. Evident but context-dependent mortality of fish passing hydroelectric turbines. Conserv Biol 2022;36(3):e13870. http://dx.doi.org/10.1111/cobi.13870, URL https://conbio.onlinelibrary.wiley.com/doi/10.1111/cobi.13870.

[19] Mueller M, Knott J, Pander J, Geist J. Experimental comparison of fish mortality and injuries at innovative and conventional small hydropower plants. J Appl Ecol 2022;59(9):2360–72. http://dx.doi.org/10.1111/1365-2664.14236, URL https://besjournals.onlinelibrary.wiley.com/doi/10.1111/1365-2664.14236.

[20] für Normung e.V. DI. DIN EN 18110:2024-08: Wasserbeschaffenheit - Verfahren zur Ermittlung der Fischdurchgängigkeit von Wasserförderschnecken, Pumpen und Spiralturbinen, die in Pumpwerken und Wasserkraftwerken verwendet werden. 2024, http://dx.doi.org/10.31030/3555890, URL https://www.dinmedia.de/de/-/-/381721727.

[21] (NEN) NN. NEN 8775:2020 fish safety - method for the determination of the fish safety of pumps, archimedean screws and confined water turbines used in pumping stations and hydroelectric plants. 2020.

[22] Čada G, Coutant C, Whitney R. Development of biological criteria for the design of advanced hydropower turbines. Idaho Fall, ID (United States): U.S. Department of Energy; 1997, http://dx.doi.org/10.2172/1218126, pages DOE/ID–100578, 1218126, 3738. Report Number: DOE/ID–100578, 1218126, 3738. URL https://www.osti.gov/servlets/purl/1218126/.

[23] Coutant CC, Whitney RR. Fish behavior in relation to passage through hydropower turbines: A review. Trans Am Fish Soc 2000;129(2):351–80. http://dx.doi.org/10.1577/1548-8659(2000)129<0351:FBIRTP>2.0.CO;2, URL http://doi.wiley.com/10.1577/1548-8659(2000)129<0351:FBIRTP>2.0.CO;2.

[24] of the Swiss Confederation TFA. Swiss animal welfare act. 2005, URL https://fedlex.data.admin.ch/eli/cc/2008/414.

[25] of the Swiss Confederation TFA. FSVO ordinance on laboratory animal husbandry, the production of genetically modified animals and methods of animal experimentation. 2010, URL https://fedlex.data.admin.ch/eli/cc/2010/207.

[26] Zangiabadi E, Masters I, Williams AJ, Croft TN, Malki R, Edmunds M, Mason-Jones A, Horsfall I. Computational prediction of pressure change in the vicinity of tidal stream turbines and the consequences for fish survival rate. Renew Energy 2017;101:1141–56. http://dx.doi.org/10.1016/j.renene.2016.09.063, URL https://linkinghub.elsevier.com/retrieve/pii/S0960148116308539.

[27] Klopries E-M, Schüttrumpf H. Mortality assessment for adult European eels (Anguilla Anguilla) during turbine passage using CFD modelling. Renew Energy 2020;147:1481–90. http://dx.doi.org/10.1016/j.renene.2019.09.112, URL https://linkinghub.elsevier.com/retrieve/pii/S0960148119314508.

[28] Stoltz U, Geiger F, Tuhtan JA. Influence of operation modes and fish behavior on fish passage through turbines. IOP Conf Ser: Earth Environ Sci 2021;774(1):012125. http://dx.doi.org/10.1088/1755-1315/774/1/012125, URL https://iopscience.iop.org/article/10.1088/1755-1315/774/1/012125.

[29] Powalla D, Hoerner S, Cleynen O, Thévenin D. A numerical approach for active fish behaviour modelling with a view toward hydropower plant assessment. Renew Energy 2022;188:957–66. http://dx.doi.org/10.1016/j.renene.2022.02.064, URL https://linkinghub.elsevier.com/retrieve/pii/S0960148122002063.

[30] Zhu G, Guo Y, Feng J, Gao L, Wu G, Luo X. Analysis and reduction of the pressure and shear damage probability of fish in a Francis turbine. Renew Energy 2022;199:462–73. http://dx.doi.org/10.1016/j.renene.2022.08.158, URL https://linkinghub.elsevier.com/retrieve/pii/S0960148122013349.

[31] Hogan TW, Cada GF, Amaral SV. The status of environmentally enhanced hydropower turbines. Fisheries 2014;39(4):164–72. http://dx.doi.org/10.1080/03632415.2014.897195, URL http://doi.wiley.com/10.1080/03632415.2014.897195.

[32] Hoerner S. Critical areas for fish passage in large axial flow pumps. In: Proceedings of the 40th IAHR world congress (vienna, 2023). Vienna; 2023.

[33] Pan Q, Weihu Z, Zhang D, Shi W, van Esch BPM. Locomotion and strike damage of fish passing through a fish friendly tubular pump using computational fluid dynamics and discrete element coupling method. Phys Fluids 2024;36(8):087129. http://dx.doi.org/10.1063/5.0216564.

[34] Ahmad F, Evans J, Nestler JM. Multiple sensor fish surrogate for acoustic and hydraulic data collection. 1997.

[35] Carlson TJ, Duncan JP. Evolution of the sensor fish device for measuring physical conditions in severe hydraulic environments. Technical report PNNL-15708, 878148, Richland, WA (United States): Pacific Northwest National Lab. (PNNL); 2003, http://dx.doi.org/10.2172/878148, URL http://www.osti.gov/servlets/purl/878148-DIWgVE/.

[36] Deng ZD, Carlson T, Duncan JP, Richmond M. Six-degree-of-freedom sensor fish design and instrumentation. Sensors 2007;7(12):3399–415. http://dx.doi.org/10.3390/s7123399, URL http://www.mdpi.com/1424-8220/7/12/3399.

[37] Deng ZD, Lu J, Myjak MJ, Martinez JJ, Tian C, Morris SJ, Carlson TJ, Zhou D, Hou H. Design and implementation of a new autonomous sensor fish to support advanced hydropower development. Rev Sci Instrum 2014;85(11). http://dx.doi.org/10.1063/1.4900543, URL http://aip.scitation.org/doi/10.1063/1.4900543.

[38] Deng ZD, Carlson TJ, Duncan JP, Richmond MC, Dauble DD. Use of an autonomous sensor to evaluate the biological performance of the advanced turbine at Wanapum Dam. J Renew Sustain Energy 2010;2(5). http://dx.doi.org/10.1063/1.3501336, URL http://aip.scitation.org/doi/10.1063/1.3501336.

[39] Fu T, Deng ZD, Duncan JP, Zhou D, Carlson TJ, Johnson GE, Hou H. Assessing hydraulic conditions through Francis turbines using an autonomous sensor device. Renew Energy 2016;99:1244–52. http://dx.doi.org/10.1016/j.renene.2016.08.029, URL https://linkinghub.elsevier.com/retrieve/pii/S0960148116307303.

[40] Martinez J, Deng ZD, Tian C, Mueller R, Phonekhampheng O, Singhanouvong D, Thorncraft G, Phommavong T, Phommachan K. In situ characterization of turbine hydraulic environment to support development of fish-friendly hydropower guidelines in the lower Mekong River region. Ecol Eng 2019;133:88–97. http://dx.doi.org/10.1016/j.ecoleng.2019.04.028, URL https://linkinghub.elsevier.com/retrieve/pii/S0925857419301454.

[41] Martinez J, Deng Z, Titzler P, Duncan J, Lu J, Mueller R, Tian C, Trumbo B, Ahmann M, Renholds J. Hydraulic and biological characterization of a large Kaplan turbine. Renew Energy 2019;131:240–9. http://dx.doi.org/10.1016/j.renene.2018.07.034, URL https://linkinghub.elsevier.com/retrieve/pii/S0960148118308310.

[42] Romero-Gomez P, Poomchaivej T, Razdan R, Robinson W, Peyreder R, Raeder M, Baumgartner LJ. Sensor fish deployments at the Xayaburi hydropower plant: Measurements and simulations. Water 2024;16(5):775. http://dx.doi.org/10.3390/w16050775, URL https://www.mdpi.com/2073-4441/16/5/775.

[43] Martinez JJ, Daniel Deng Z, Klopries E-M, Mueller RP, Scott Titzler P, Zhou D, Beirao B, Hansten AW. Characterization of a siphon turbine to accelerate low-head hydropower deployment. J Clean Prod 2019;210:35–42. http://dx.doi.org/10.1016/j.jclepro.2018.10.345, URL https://linkinghub.elsevier.com/retrieve/pii/S0959652618333821.

[44] Pauwels IS, Baeyens R, Toming G, Schneider M, Buysse D, Coeck J, Tuhtan JA. Multi-species assessment of injury, mortality, and physical conditions during downstream passage through a large archimedes hydrodynamic screw (Albert Canal, Belgium). Sustainability 2020;12(20):8722. http://dx.doi.org/10.3390/su12208722, URL https://www.mdpi.com/2071-1050/12/20/8722.

[45] Knott J, Mueller M, Pander J, Geist J. Ecological assessment of the world's first shaft hydropower plant. Renew Sustain Energy Rev 2023;187:113727. http://dx.doi.org/10.1016/j.rser.2023.113727, URL https://linkinghub.elsevier.com/retrieve/pii/S1364032123005841.

[46] Brown RS, Pflugrath BD, Colotelo AH, Brauner CJ, Carlson TJ, Deng ZD, Seaburg AG. Pathways of barotrauma in juvenile salmonids exposed to simulated hydroturbine passage: Boyle's law vs. Henry's law. Fish Res 2012;121–122:43–50. http://dx.doi.org/10.1016/j.fishres.2012.01.006, URL https://linkinghub.elsevier.com/retrieve/pii/S0165783612000379.

[47] Kerr JR, White PR, Leighton TG, Silva LGM, Kemp PS. Boyle's Law ignores dynamic processes in governing barotrauma in fish. Sci Rep 2023;13(1):19125. http://dx.doi.org/10.1038/s41598-023-46125-9, URL https://www.nature.com/articles/s41598-023-46125-9.

[48] Geiger F, Cuchet M, Peter R. Zur Verringerung von Fischschäden in Turbinen mittels Verhaltensbeeinflussung. WASSERWIRTSCHAFT 2020;110(12):41–5. http://dx.doi.org/10.1007/s35147-020-0756-5, URL https://www.springerprofessional.de/doi/10.1007/s35147-020-0756-5.

[49] Vowles AS, Kemp PS. Effects of light on the behaviour of brown trout (Salmo trutta) encountering accelerating flow: Application to downstream fish passage. Ecol Eng 2012;47:247–53. http://dx.doi.org/10.1016/j.ecoleng.2012.06.021, URL https://linkinghub.elsevier.com/retrieve/pii/S0925857412002200.

[50] Cox RX, Felder S. Injury-free transport of fish through closed conduit components. J Ecohydraulics 2025;1–16. http://dx.doi.org/10.1080/24705357.2025.2462296, URL https://www.tandfonline.com/doi/full/10.1080/24705357.2025.2462296.

[51] Deng ZD, Guensch GR, McKinstry CA, Mueller RP, Dauble DD, Richmond MC. Evaluation of fish-injury mechanisms during exposure to turbulent shear flow. Can J Fish Aquat Sci 2005;62(7):1513–22, Publisher: NRC Research Press Ottawa, Canada.

[52] Richmond MC, Deng ZD, McKinstry CA, Mueller RP, Carlson TJ, Dauble DD. Response relationships between Juvenile Salmon and an autonomous sensor in turbulent flow. Fish Res 2009;97(1–2):134–9. http://dx.doi.org/10.1016/j.fishres.2009.01.011, URL https://linkinghub.elsevier.com/retrieve/pii/S016578360900040X.

[53] Bercovitz Y, Tissot L, Sagnes P, Courret D, Lebert F, Lagarigue T, Mataix V, Dumond L. Evaluation of fish injuries at the outlet of downstream passage devices: Preliminary in situ and laboratory experiments with Sensor Fish. In: Proceedings of the 39th IAHR world congress. International Association for Hydro-Environment Engineering and Research (IAHR); 2022, p. 1237–45. http://dx.doi.org/10.3850/IAHR-39WC25217119202255, URL https://www.iahr.org/library/infor?pid=20868.

[54] Hoerner S, Kösters WI, Abbaszadeh S, Wagner F, Tuhtan JA. Towards a reliable and validated toolbox to replace live fish tests for the assessment of injury and mortality during downstream passage. In: IAHR 15th international symposium on ecohydraulics and fish passage. Quebec City, Canada; 2024, URL https://hal.science/hal-04642604.

[55] Hou H, Deng ZD, Martinez J, Fu T, Duncan JP, Johnson G, Lu J, Skalski J, Townsend R, Tan L. A hydropower biological evaluation toolset (HBET) for characterizing hydraulic conditions and impacts of hydro-structures on fish. Energies 2018;11(4):990. http://dx.doi.org/10.3390/en11040990, URL http://www.mdpi.com/1996-1073/11/4/990.

[56] Salalila A, Deng ZD, Martinez JJ, Lu J, Baumgartner LJ. Evaluation of a fish-friendly self-cleaning horizontal irrigation screen using autonomous sensors. Mar Freshwater Res 2019;70(9):1274. http://dx.doi.org/10.1071/MF19194, URL http://www.publish.csiro.au/?paper=MF19194.

[57] Turnpenny AWH, Davis MH, Flemming JM, Davies JK. Experimental studies relating to the passage of fish and shrimps through tidal power turbines. Mar Freshw Res Unit, Natl Power 1992.

[58] Amaral SV, Hecker GE. Evaluation of the effects of turbine blade leading edge design on fish survival. Electr Power Res Inst 2008;(1014937).

[59] Bevelhimer MS, Pracheil BM, Fortner AM, Saylor R, Deck KL. Mortality and injury assessment for three species of fish exposed to simulated turbine blade strike. Can J Fish Aquat Sci 2019;76(12):2350–63. http://dx.doi.org/10.1139/cjfas-2018-0386, URL http://www.nrcresearchpress.com/doi/10.1139/cjfas-2018-0386.

[60] Saylor RK, Fortner A, Bevelhimer M. Quantifying mortality and injury susceptibility for two morphologically disparate fishes exposed to simulated turbine blade strike. Hydrobiologia 2019;842(1):55–75. http://dx.doi.org/10.1007/s10750-019-04026-x, URL http://link.springer.com/10.1007/s10750-019-04026-x.

[61] Saylor RK, Sterling D, Bevelhimer M, Pracheil B. Within and among fish species differences in simulated turbine blade strike mortality: Limits on the use of surrogacy for untested species. Water 2020;12(3):701. http://dx.doi.org/10.3390/w12030701, URL https://www.mdpi.com/2073-4441/12/3/701.

[62] Meng L, Chen R, Wang X, Zhang CY, Zheng Y, Tian YJ. Turbine blade strike tests for evaluation and optimization of fish-friendly turbine. IOP Conf Ser: Earth Environ Sci 2022;1037(1):012058. http://dx.doi.org/10.1088/1755-1315/1037/1/012058, URL https://iopscience.iop.org/article/10.1088/1755-1315/1037/1/012058.

[63] Bevelhimer MS, Pracheil BM, Fortner AM, Deck KL. An overview of experimental efforts to understand the mechanisms of fish injury and mortality caused by hydropower turbine blade strike. Technical Report ORNL/TM-2017/731, 1425338, Oak Ridge, TN (United States): Oak Ridge National Laboratory (ORNL); 2017, http://dx.doi.org/10.2172/1425338, URL http://www.osti.gov/servlets/purl/1425338/.

[64] Hecker GE, Amaral SV, Stacy PS. Investigation of hydro-turbine leading-edge shapes favorable to fish survival. Technical Report 102561, Palo Alto, CA: Electric Power Research Institute; 2007.

[65] Saylor RK, Bevelhimer M, Pracheil B. Fish injury and mortality caused by simulated impacts from turbine blades. 2020, http://dx.doi.org/10.21951/1755094, URL https://www.osti.gov/servlets/purl/1755094/.

[66] Saylor RK, Wang PL, Bevelhimer M, Lloyd P, Goodwin J, Laughter R, Young D, Sterling D, Mhatre P, Atkins C, Post B. Creation of a prototype biomimetic fish to better understand impact trauma caused by hydropower turbine blade strikes. PeerJ Mater Sci 2021;3. http://dx.doi.org/10.7717/peerj-matsci.16, URL https://peerj.com/articles/matsci-16.

[67] Leys C, Ley C, Klein O, Bernard P, Licata L. Detecting outliers: Do not use standard deviation around the mean, use absolute deviation around the median. J Exp Soc Psychol 2013;49(4):764–6. http://dx.doi.org/10.1016/j.jesp.2013.03.013, URL https://www.sciencedirect.com/science/article/pii/S0022103113000668.

[68] Leys C, Delacre M, Mora YL, Lakens D, Ley C. How to classify, detect, and manage univariate and multivariate outliers, with emphasis on pre-registration. Int Rev Soc Psychol 2019;32(1). http://dx.doi.org/10.5334/irsp.289, URL https://rips-irsp.com/articles/10.5334/irsp.289.

[69] Abbaszadeh S, Hoerner S, Leidhold R. Experimental optimization of a fish robot's swimming modes: A complex multiphysical problem. Exp Fluids 2024;65(4):51. http://dx.doi.org/10.1007/s00348-024-03786-0, URL https://link.springer.com/10.1007/s00348-024-03786-0.

[70] Pflugrath BD, Saylor R, Engbrecht KM, Mueller RP, Stephenson JR, Bevelhimer M, Pracheil BM, Colotelo AH. Biological response models: Predicting injury and mortality of fish during downstream passage through hydropower facilities. Technical Report PNNL-30893, Pacific Northwest National Lab. (PNNL), Richland, WA (United States); 2021, http://dx.doi.org/10.2172/1838202, URL https://www.osti.gov/biblio/1838202.

[71] Kösters WI, Tuhtan J, Efimov D, Kruusmaa M, Hoerner S. CAD data: An open laboratory blade strike rig to evaluate the risk of injury and mortality to fish and to test passive sensors. 2025, http://dx.doi.org/10.5281/ZENODO.15078947, URL https://zenodo.org/doi/10.5281/zenodo.15078947.

[72] Pauwels IS, Broos S, Vandamme L, Van Wichelen J, Coeck J, Toming G, Tuhtan JA, Buysse D. A fish-friendly axial flow pump turns out to be eel safe, roach unfriendly and bream unsafe. Sci Rep 2024;14(1):30234. http://dx.doi.org/10.1038/s41598-024-81095-6, URL https://www.nature.com/articles/s41598-024-81095-6.

[73] Kösters WI. Supplementary Data: An open laboratory blade strike rig to evaluate the risk of injury and mortality to fish and to test passive sensors. 2025, http://dx.doi.org/10.5281/ZENODO.15864853, URL https://zenodo.org/doi/10.5281/zenodo.15864853.

[74] Kösters WI, Efimov D. Figure data: An open laboratory blade strike rig to evaluate the risk of injury and mortality to fish and to test passive sensors. 2025, http://dx.doi.org/10.5281/ZENODO.15078904, URL https://zenodo.org/doi/10.5281/zenodo.15078904.